J Forensic Sci, September 2003, Vol. 48, No. 5
Paper ID JFS2002385_485
Available online at: www.astm.org

Che-Yen Wen,[1] *Ph.D. and Chiu-Chung Yu,*[1] *M.S.*

Fingerprint Pattern Restoration by Digital Image Processing Techniques*

ABSTRACT: Fingerprint evidence plays an important role in solving criminal problems. However, defective (lacking information needed for completeness) or contaminated (undesirable information included) fingerprint patterns make identifying and recognizing processes difficult. Unfortunately, this is the usual case. In the recognizing process (enhancement of patterns, or elimination of "false alarms" so that a fingerprint pattern can be searched in the Automated Fingerprint Identification System (AFIS)), chemical and physical techniques have been proposed to improve pattern legibility. In the identifying process, a fingerprint examiner can enhance contaminated (but not defective) fingerprint patterns under guidelines provided by the Scientific Working Group on Friction Ridge Analysis, Study and Technology (SWGFAST), the Scientific Working Group on Imaging Technology (SWGIT), and an AFIS working group within the National Institute of Justice. Recently, the image processing techniques have been successfully applied in forensic science. For example, we have applied image enhancement methods to improve the legibility of digital images such as fingerprints and vehicle plate numbers.

In this paper, we propose a novel digital image restoration technique based on the AM (amplitude modulation)-FM (frequency modulation) reaction-diffusion method to restore defective or contaminated fingerprint patterns. This method shows its potential application to fingerprint pattern enhancement in the recognizing process (but not for the identifying process). Synthetic and real images are used to show the capability of the proposed method. The results of enhancing fingerprint patterns by the manual process and our method are evaluated and compared.

KEYWORDS: forensic science, fingerprints, AM-FM reaction-diffusion, image restoration

Fingerprints are the oldest and most extensively studied biometric technique of identification (1). The procedures for processing latent fingerprint patterns are shown in Fig. 1. The figure represents the systematic approaches used in the forensic science laboratory. If the fingerprints from criminal scenes can be obviously verified, we can obtain them directly by applying visible light and photographing. In the recognizing process (enhancement of patterns, or elimination of "false alarms" so that a fingerprint pattern can be searched in AFIS), instrumental methods (for example, UV absorption and reflection, the laser method, . . . etc.), physical methods (for example, powdering, small particle reagent, vacuum metal deposition, . . . etc.), and chemical methods (ninhydrin and its analogues, DFO, cyanoacrylate, . . . etc.) have been proposed to improve pattern legibility. In the identifying process, a fingerprint examiner can enhance contaminated (but not defective) fingerprint patterns under guidelines provided by SWGFAST, SWGIT, and an AFIS working group within the National Institute of Justice. After these procedures, the pre-processed fingerprint patterns are identified by AFIS. To explain the process of "elimination for undesirable information," we use Fig. 2 as an example. In Fig. 2*a*, we can see many "false alarm" features being generated by AFIS. In Fig. 2*b*, the image after the process of elimination for undesirable information, we can see the "false alarm" features being eliminated.

The image processing techniques have been successfully applied in forensic science. For a fingerprint pattern image of poor clarity, image enhancement methods have been proposed to improve the legibility of fingerprints (2–4). These enhancement methods can be classified as spatial (image) domain and frequency domain methods. Spatial domain techniques (such as Sobel filters, Pratt filters, . . . etc.) are used to remove additive noise from fingerprint images. For frequency domain methods, digital images can be represented as a collection of different frequency components (energy spectra). The transform used to perform conversion from the spatial domain to the frequency domain is known as the discrete Fourier transform (DFT). Enhancement can be achieved by adjusting particular frequency components that are with the interested information. Recently, the wavelet transform (WT) is used to reduce the noise and enhance the information of contaminated images. WT belongs to the so-called the time-scale domain method (combination of spatial and frequency). These methods (spatial, frequency, and time-scale domain) can improve the visual quality of fingerprint images.

The AM-FM reaction-diffusion method has been used to complete defective and occluded oriented image textures (5). The method uses AM-FM models to characterize image textures (i.e., estimation of texture parameters). With the estimated parameters, we can use the AM-FM model to represent image textures and reconstruct them via the reaction and diffusion process.

In this paper, we propose a novel digital image restoration technique based on the AM-FM reaction-diffusion method to restore defective or contaminated fingerprint patterns. This method shows its potential application to fingerprint pattern enhancement in the recognizing process (but not for the identifying process). Synthetic and real images are used to show the capability of the proposed method. The results of enhancing fingerprint patterns by the manual process and our method are evaluated and compared.

[1] Department of Forensic Science, Central Police University, Taoyuan, Taiwan.

* This work was supported by National Science Council, Taiwan (NSC91-2213-E-015-001).

Received 2 Nov. 2002; and in revised form 15 Mar. 2003; accepted 15 March 2003; published 4 Aug. 2003.

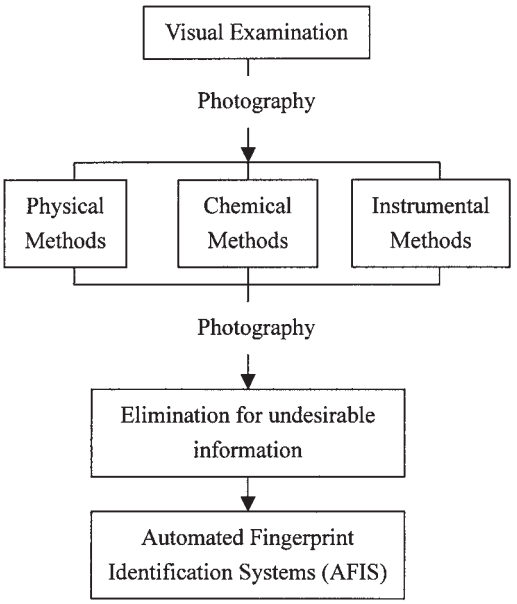

FIG. 1—*The procedures for processing latent fingerprint patterns.*

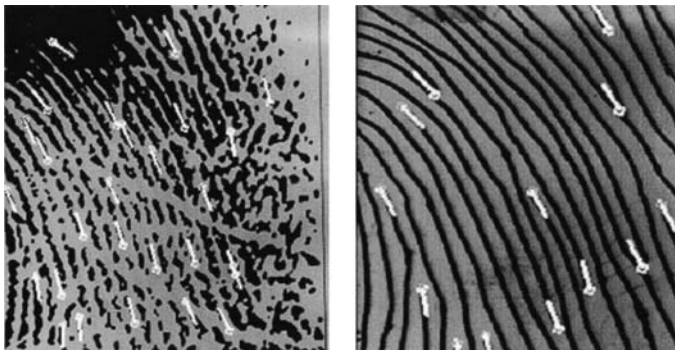

FIG. 2—*An example of "elimination for undesirable information" (see Fig. 1); the symbols show the feature positions detected by AFIS: (a) the original image; we can see many "false alarm" features being generated; (b) the image after the process of elimination for undesirable information; we can see the "false alarm" features being eliminated.*

Methods

In order to analyze universal image statistics, Zhu and Mumford proposed a new class of Gibbs distributions of the following form (6):

$$p(I;\Lambda;S) = \frac{1}{Z}\, e^{-U(I;\Lambda;S)} \tag{1}$$

$$U(I;\Lambda;S) = \sum_{\alpha=1}^{K} \sum_{(x,y)} \lambda^{(\alpha)}((F^{(\alpha)} * I)(x,y)) \tag{2}$$

where I is an image, Z is a normalization factor, $S = \{F^{(1)}, F^{(2)}, \ldots, F^{(K)}\}$ is a set of linear filters, and $\Lambda = \{\lambda^{(1)}(), \lambda^{(2)}(), \ldots \lambda^{(K)}()\}$ is a set of potential functions. They argue that random samples from these models can duplicate very general classes of textures for an appropriate choice of a set of filters S. The potential functions $\Lambda = \{\lambda^{(1)}(), \lambda^{(2)}(), \ldots \lambda^{(K)}()\}$ can be classified into two categories: diffusion process terms and reaction process terms. The diffusion process produces denoising effects, while the reaction process forms patterns and enhances image features. The typical potential functions lead to image smoothing via anisotropic diffusion. Inverted potential functions produce pattern formation or reaction. This kind of reaction-diffusion process has been employed to produce oriented patterns such as leopard blobs and zebra stripe (7,8).

From Ref 5, the reaction-diffusion mechanism used for texture reconstruction can be described by the following equation:

$$\frac{\partial I}{\partial t} = \rho_D D + \rho_R R \tag{3}$$

where I is an image, D is the diffusion term, R is the reaction term, ρ_D is the rate of diffusion, and ρ_R is the rate of reaction. For an image $I(X)$, where $X = (x, y)$ is the location, we can rewrite Eq 3 as

$$\frac{\partial I_t(X)}{\partial t} = \rho_D(X)\, D(X) + \rho_R(X)\, R(X) \tag{4}$$

where $I_t(X)$ is the intensity of location X at iteration t. $\rho_D(X)$, $\rho_R(X)$, $D(X)$ and $R(X)$ are location-variant (location dependent). In the digital (discrete) image case, Eq 4 can be implemented by

$$I_{t+1}(X) \leftarrow I_t(X) + \rho_D(X)D(X) + \rho_R(X)R(X) \tag{5}$$

where $I_t(X)$ is the intensity of location X at iteration t. For the perfect regions (with complete patterns) of the image, the initial image intensities on $I_0(X)$ are equal to those on the input image $I(X)$. From Eqs 5 and 6, "seed" the reaction-diffusion process with uniform noises or noises that are distributed identically to the surrounding region. Unfortunately, this noise-based mode is not suitable for fingerprint patterns, since fingerprint patterns are not random noises. In our method, we "seed" the reaction-diffusion process with the information of perfect image regions.

Based on Eq 5, we can define the diffusion and reaction processes. Diffusion and reaction processes have conflicting objectives (5). The goal of the diffusion process is to smooth image patterns and eliminate noises, while the goal of the reaction process is to form pattern edge contours.

Diffusion Process

We define the diffusion term $D(X)$ of Eq 5. An anisotropic diffusion equation is introduced as

$$\frac{\partial I_t(X)}{\partial t} = div\{c(X,t)\nabla I_t(X)\} \tag{6}$$

where $X = (x, y)$ is the location on an image, $I_0(X)$ is the input image, $\nabla I_t(X)$ is the image gradient, $c(X, t)$ is the diffusion coefficient, and $div[\cdot]$ is the divergence operator and defined as

$$div(\overline{V}) = \nabla_x P + \nabla_y Q \tag{7}$$

For a vector $\overline{V} = (P, Q)$, $\nabla_x P$ is the gradient along the x axis; $\nabla_y Q$ is the gradient along the y axis (9,10). The equivalent discrete representation of Eq 6 for substitution in Eq 5 (i.e. $D(X)$) is given by

$$D(X) = \sum_{d=1}^{\Gamma} c_d(X)\nabla I_d(X) \tag{8}$$

where $c_d(X)$ is the diffusion coefficient, Γ is the number of directions in which diffusion is computed, and $\nabla I_d(X)$ is the directional gradient in direction d at location X (10). For example, $\Gamma = 4$, $\nabla I_d(X)$ is the directional gradient with respect to the "western," "eastern," "northern," and "southern" neighbors. If $X = (x,y)$ and

$d = 1$, $\nabla I_1(x) = I(x - h_1, y) - I(x, y)$, the parameter h_1 defines the sampling interval length.

The most important step to design the diffusion process is the proper selection of the diffusion coefficient $c_d(X)$. From Eq 10, we can define the diffusion coefficient as

$$c_d(X) = exp\left\{-\left[\frac{\nabla S_d(X)}{k}\right]^2\right\} \quad (9)$$

A B

FIG. 3—*Edge detection by the morphological anisotropic diffusion method*: *(a) a fingerprint image*; *(b) the result of edge detection.*

and

$$S_d = (I \circ B) \cdot B \quad (10)$$

where k is a scaling constant, B is a structuring element of size $m \times m$, $I \circ B$ is the morphological opening of I by B, and $I \cdot B$ is the morphological closing of I by B (11).

The selection of the diffusion coefficient, $c_d(X)$, is the key point in the diffusion process. The anisotropic diffusion is used to inhibit smoothing at image edges, and it is also used to develop the edge detection technique. Figure 3 shows an example of edge detection with the morphological anisotropic diffusion method, and Fig. 4 shows that the morphological anisotropic diffusion method can be used to eliminate noise and preserve edges.

In this paper, we use the discrete version of the anisotropic diffusion (12). From Eqs 5 and 8, the image intensities are updated according to:

$$I_{t+1}(X) \leftarrow I_t(X) + \rho_D(X)\, D(X) \quad (11)$$

where $\rho_D(X)$ is the rate of diffusion, $\rho_D(X) \leq 1/2$ is for the one-dimensional $D(X)$, and $\rho_D(X) \leq 1/4$ is for the two-dimensional case (four diffusion directions).

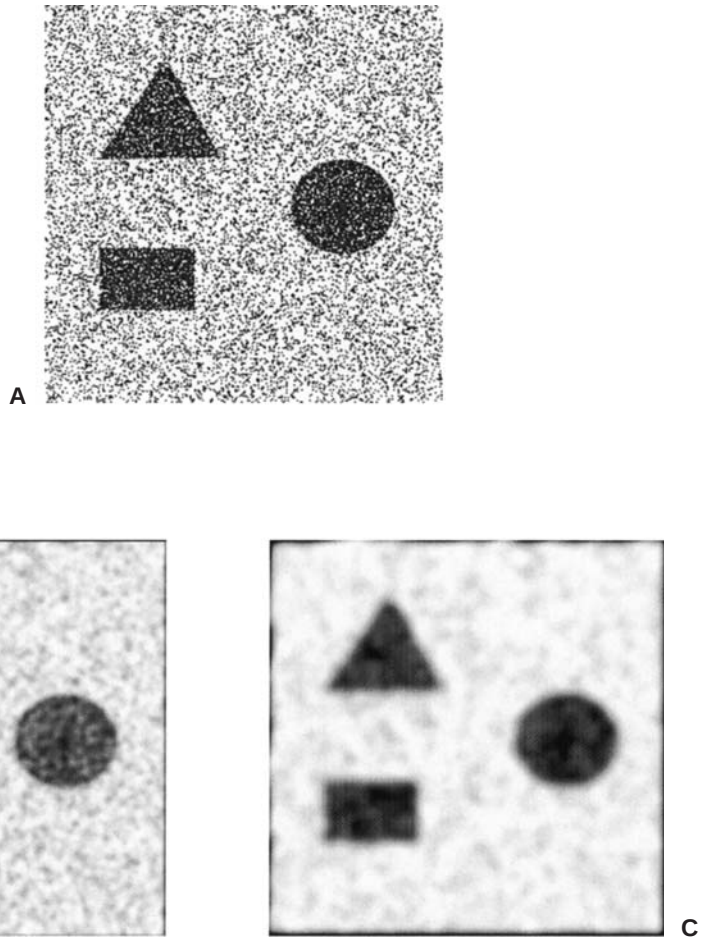

A B C

FIG. 4—*An example of eliminating noises and preserving edges with the morphological anisotropic diffusion method*: *(a) an image corrupted with salt-pepper noises*; *(b) after twelve iterations of morphology anisotropic diffusion with Eq 9; k = 128*; *(c) after 24 iterations of morphology anisotropic diffusion; k =128.*

Reaction Process

In this subsection, we define the reaction term $R(X)$ of Eq 5. The reaction process encourages formation of patterns of directionality. To produce patterns that correspond to oriented texture features, the reaction term is given by Eqs 5 and 6.

$$R(X) = G_x \otimes [\varphi(G_X * I)] \tag{12}$$

where G_x is the Gabor filter (Eq 14), which is designed to produce the specific texture orientation at position X. The operator "$\otimes$" is the correlation operator and "$*$" is the convolution operator (11). The function $\varphi(\cdot)$ weights the contribution of the Gabor filter, and it is defined as (Eq 6)

$$\varphi(\gamma) = -\left(1 - \frac{1}{1+(|\gamma|/k)^2}\right) \tag{13}$$

where k is a scaling constant. In the case of the fingerprint pattern generation, we can set k according to the desired contrast within the fingerprint. For an 8-bit gray-level-valued image, we can set $k = 255$.

The Gabor filter (Fig. 5 shows an example) is applied extensively in image processing, such as pattern segmentation, texture classification, and image recognition. The Gabor filter G is given by a cosine function and a two-dimensional Gaussian function $g_\sigma(x, y)$:

$$G = \cos[(2\pi/M)(ux+vy)] \cdot g_\sigma(x, y) \tag{14}$$

where M is a constant used to control the cycle of patterns, u and v are the horizontal and vertical frequency, and σ is the standard deviation of the Gaussian function $g_\sigma(x, y)$. In fingerprint pattern, one cycle includes a ridge and its neighbor valley. The Gabor parameters (u, v) are automatically determined by the AM-FM model (we will discuss it later).

With the reaction process, we can create some "natural" image patterns. Using a pepper noise image as the initial image and with Eq 12 we can obtain "zebra stripes" patterns (Fig. 6*a*). If we replace the Gabor filter with the Gaussian filter, we can obtain "blood cell" patterns (Fig. 6*b*).

Rate of Reaction-Diffusion

The rates, $\rho_R(X)$ and $\rho_D(X)$, of Eq 5 are important factors affecting the implementation of reaction-diffusion for texture restoration. We will discuss how to determine $\rho_R(X)$ and $\rho_D(X)$ in this subsection.

Let Ω denote the domain of an image, $U \subset \Omega$ denotes the region with complete patterns in the image, and $B \subset \Omega$ denotes the region with defective patterns in the image. Since the objectives of processing within the complete region U and the defective region B are different, we let $\rho_R(X)$ and $\rho_D(X)$ vary with location X. In order to provide simultaneous enhancement and smoothness between U and B, we process the diffusion within the entire complete region U. The reaction operator is also performed on the boundaries between U and B to guarantee pattern matching within the boundary region.

The rate of reaction $(\rho_R(X))$ is determined by the maximum number of iterations, which is determined by

$$\rho_R(X) = \frac{\sum_{(x,y)\in W} I(x,y)}{N^2 \cdot k} \tag{15}$$

where N^2 = the number of pixels in the localized area W, and k is a scaling constant (same as in Eq 13).

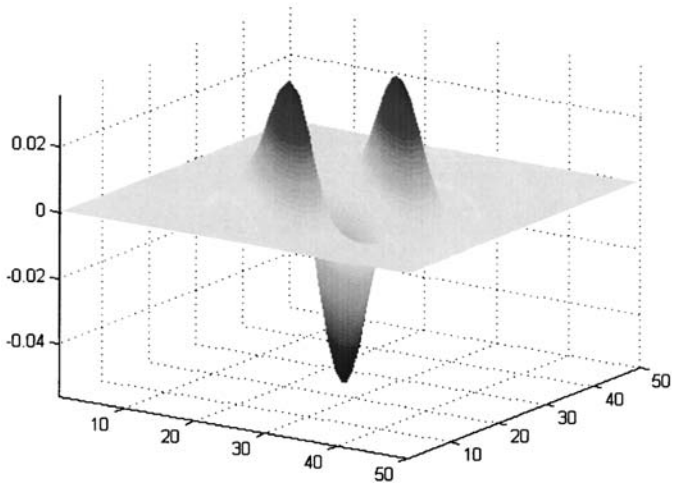

FIG. 5—*A 3-D mesh plot of the Gabor filter.*

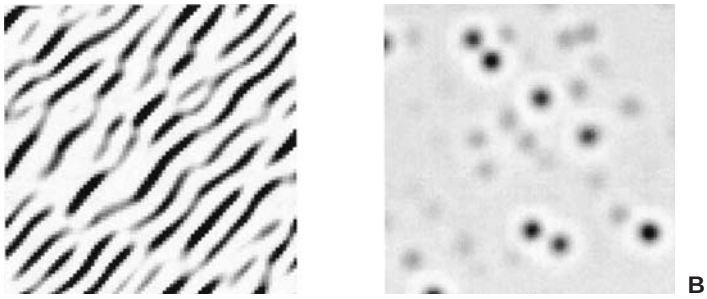

FIG. 6—*Patterns produced by the reaction process*: *(a) a "zebra stripes" image*; *(b) a "blood cells" image.*

For the rate of diffusion $(\rho_D(X))$, if $X \in B$, we let

$$\rho_D(X) \leq ¼ \tag{16}$$

for stability; if $X \in U$, we let

$$\rho_D(X) = \frac{1}{4}\varepsilon \tag{17}$$

where ε is a constant. In this paper, we use $\varepsilon = 0.1$. ε is determined by two requirements: (1) the generated patterns need to fit the existing boundaries between U and B, (2) distortion made in region U must be minimized.

Appropriate reaction filters for reconstructing the texture patterns are the key points to the success of the reaction-diffusion model. In this paper, we utilize an AM-FM model to derive the filter parameters for the defective regions in the image.

AM-FM Model

The AM-FM model has been used to model textured images (13,14) and to analyze human speech signals (15–18). With joint amplitude-frequency modulated AM-FM components, we can obtain the characteristics of a texture image and duplicate the image. Each AM-FM component is composed of two functions—AM and FM function. The AM function may be interpreted as the instantaneous intensity variation, while the FM function denotes the vector-valued derivative of the instantaneous phase and describes the local texture orientation.

For a given image, the demodulation process deals with the computation of the AM and FM functions. The AM and FM functions provide an extensive description of the local texture structure. Those functions can be used to texture analysis (19,20), texture segmentation, classification, and reconstructing (5,21). Since the AM-FM functions are with complex models, we need a complex-valued transform when applying AM-FM functions to real-valued signals (e.g., images). This is why we need the Hilbert transform.

Hilbert Transform

Hilbert transform is used to define the complex-valued analytic image associated with a real-valued image. The extension of the transformed image is called the *analytic image* (22). The properties of Hilbert transform can be reviewed in Refs 22–25.

Gabor (23) defined the amplitude and frequency of a one-dimensional real-valued signal $s(x)$ in terms of a complex-valued signal, called the analytic signal $z(x)$, which is defined by $z(x) = s(x) + jc(x)$, where

$$c(x) = H[s(x)] = s(x) * \frac{1}{\pi x} = \frac{1}{\pi}\int_R \frac{s(\tau)}{x-\tau}\,d\tau \qquad (18)$$

is the Hilbert transform $H[\cdot]$ of the original real-valued signal $s(x)$.

For a $N \times M$ real-valued image $f(x, y)$, its analytic image $(z(x, y))$ is given by $z(x, y) = f(x, y) + jg(x, y)$, where $g(x, y)$ is the 2-D Hilbert transform of $f(x, y)$. We can also write the analytic image in the frequency domain format, $Z(u, v) = F(u, v) + jG(u, v)$, where $Z(u, v)$, $F(u, v)$, and $G(u, v)$ are the discrete Fourier transforms of $z(x, y)$, $f(x, y)$, and $g(x, y)$, respectively.

$z(x, y)$ can be computed by the following straightforward procedure. Since $G(u, v) = H(u, v) \cdot F(u, v)$ (Eq 19), where

$$H(u,v) = \begin{cases} & u = 1,2,\ldots,\dfrac{N}{2}-1 \\ -j, & u = \dfrac{N}{2}+1,\dfrac{N}{2}+1,\ldots,N-1 \\ j, & u = 0,\ v = 1,2,\ldots,\dfrac{M}{2}-1 \\ -j, & \\ -j, & u = \dfrac{N}{2},\ v = 1,2,\ldots,\dfrac{M}{2}-1 \\ j, & u = 0,\ v = \dfrac{M}{2}+1,\dfrac{M}{2}+2,\ldots,M-1 \\ j, & \\ 0, & u = \dfrac{N}{2},\ v = \dfrac{M}{2}+1,\dfrac{M}{2},\ldots M-1 \\ & \text{otherwise} \end{cases} \qquad (19)$$

We can obtain $Z(u, v) = F(u, v) + jG(u, v)$ easily. $z(x, y)$ can be obtained by taking the inverse DFT of $Z(u, v)$. Figure 7 shows a "diamond image," its Hilbert transform, and estimated AM-FM functions.

Restoration of the Oriented Texture

A signal $f(k)$ can be modeled as a single AM-FM function,

$$f(k) = a(k)\cos[\varphi(k)] = \mathrm{Re}\{a(k)\exp[j\varphi(k)]\} \qquad (20)$$

where $a(k)$ denotes the AM function and $\varphi(k)$ denotes the FM function. However, single-component modulation models are rarely appropriate for modeling real-world images. Suppose that $f(n_1, n_2)$ is an $N \times M$ image, where n_1 and n_2 are integer, $0 \le n_1 \le N$ and $0 \le$

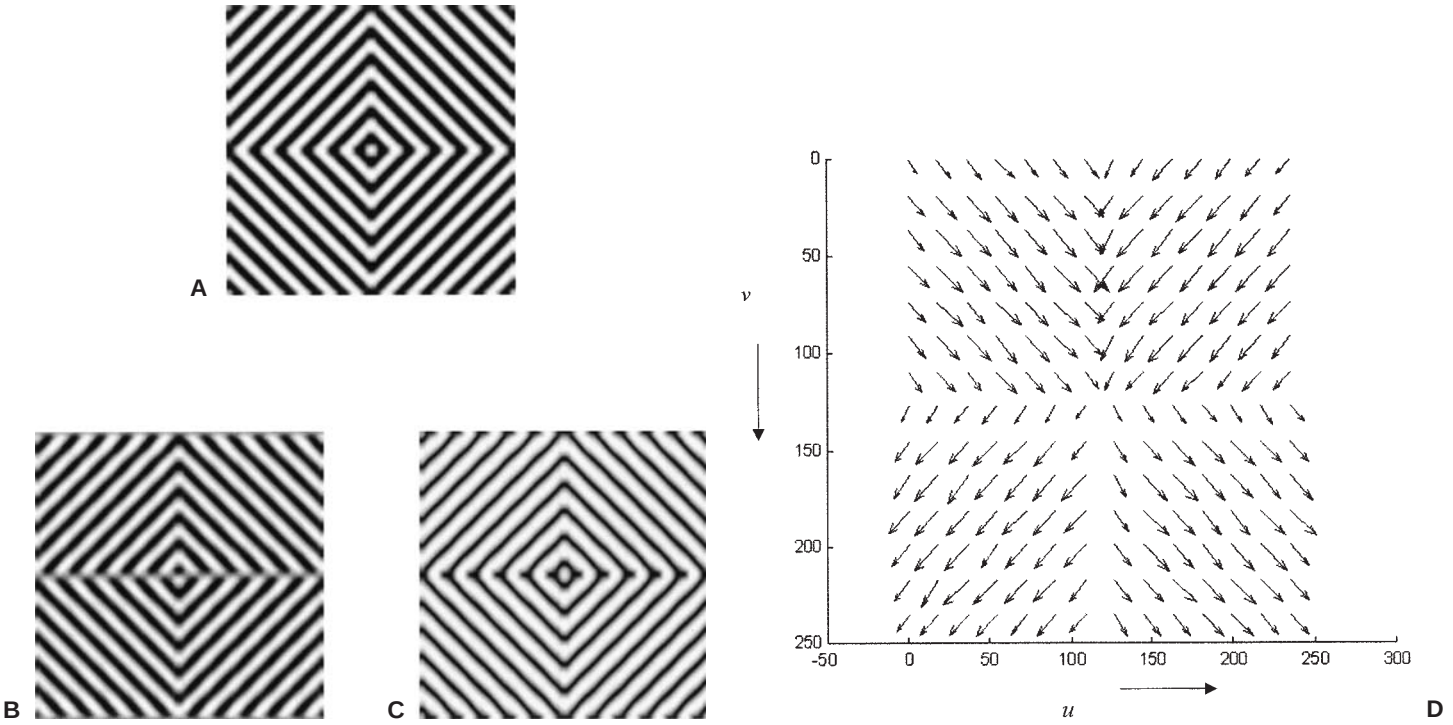

FIG. 7—*An AM-FM synthetic image example*: *(a) the synthetic diamond image*; *(b) the Hilbert transform of (a)*; *(c) the AM function a(x,y) estimated by Eq 24*; *(d) the FM function (frequency vectors) estimated by using Eqs 25–28, each arrow (vector) is in the direction* $\arctan[|v(x, y)|/|u(x, y)|]$.

$n_2 \leq M$. If $f(n_1, n_2)$ takes real floating point values, we can model the image according to

$$f(n_1, n_2) = a(n_1, n_2) \cos[\varphi(n_1, n_2)] \quad (21)$$

We also assume that $f(n_1, n_2)$ contains the samples of a continuous image,

$$f_c(n_1, n_2) = a_c(n_1, n_2) \cos[\varphi_c(n_1, n_2)] \quad (22)$$

$\nabla[\varphi_c(n_1, n_2)]$ is defined as the instantaneous frequency of $f_c(n_1, n_2)$. By definition, $\nabla[\varphi_c(n_1, n_2)]$ is the FM function of $f_c(n_1, n_2)$ in Eq 22. This quantity is a vector with components $\partial\varphi_c(n_1, n_2)/\partial n_1$ and $\partial\varphi_c(n_1, n_2)/\partial n_2$, which are referred to, respectively, as the horizontal and vertical instantaneous frequencies. In an image, the single-component demodulation problem is to estimate AM function ($\hat{a}(n_1, n_2)$) and FM function ($\hat{\varphi}(n_1, n_2)$) such that $f(n_1, n_2) \approx \hat{a}(n_1, n_2) \cos[\hat{\varphi}(n_1, n_2)]$. The first procedure is to demodulate $f(n_1, n_2)$ by a well-defined algorithm that uses the real values of the image to calculate a complex extension $z(n_1, n_2) = f(n_1, n_2) + jg(n_1, n_2)$. The second procedure is to estimate AM and FM functions from $z(n_1, n_2)$. These two procedures are described in the next subsection.

Demodulation by Complex Extension

We describe a technique that estimates the AM and FM functions of a real-valued single-component image by computing a complex-valued extension of the image and demodulating the complex image (5). The particular complex extension is called the *analytic image.* It is very advantageous to write complex signals

$$\begin{aligned} z(x, y) &= I(x, y) + jg(x, y) \\ &= a(x, y)e^{j\Phi(x, y)} \end{aligned} \quad (23)$$

where $z(x, y)$ is constructed by adding an imaginary part $g(x, y)$ to the real image $I(x, y)$, and $g(x, y)$ is the Hilbert transform of $I(x, y)$. $a(x, y)$ denotes the AM function and $\phi(x, y)$ denotes the FM function. In practice, the estimated AM function (Eq 24) and FM function (Eqs 25–28) can be obtained by using the following algorithms (26):

$$a(x, y) = |z(x, y)| \quad (24)$$

$$|u(x, y)| = \arccos\left[\frac{z(x + 1, y) + z(x - 1, y)}{2z(x, y)}\right] \quad (25)$$

$$\text{sgn } u(x, y) = \text{sgn arcsin}\left[\frac{z(x + 1, y) - z(x-1, y)}{2z(x, y)}\right] \quad (26)$$

$$\arccos\left[\frac{z(x, y + 1) + z(x, y - 1)}{2z(x, y)}\right] \quad (27)$$

$$\arcsin\left[\frac{z(x, y + 1) - z(x, y-1)}{2\,jz(x, y)}\right] \quad (28)$$

A synthetic image example is shown in Fig. 7. Figure 7*a* is the synthetic diamond image, Fig. 7*b* is the Hilbert transform of the diamond image, Fig. 7*c* is the AM function $a(x, y)$ estimated by Eq 24, and Fig. 7*d* is the FM function (frequency vectors) estimated by using Eqs 25–28. In Fig. 7*d*, each arrow (vector) is in the direction $[\,|v(x, y)|\,/\,|u(x, y)|\,]$.

The Parameters of Component Selection

The component parameter selection technique is used for estimation of the AM and FM functions. In Eqs 12 and 14, the Gabor parameters (u, v) play important roles in the reaction term. They affect the orientation and cycle of produced patterns. In Eqs 25–28, the FM function is formed by $u(x, y)$ and $v(x, y)$. The functions $u(x, y)$ and $v(x, y)$ are the horizontal and vertical instantaneous frequencies of $z(x, y)$, respectively. Here, we analyze the FM function and get the useful parameters for the reaction term.

Figure 8*a* is an original fingerprint image with similar oriented patterns, and Fig. 8*b* is the preprocessed image of Fig. 8*a*. We will use this image sample to show the capability of our method. Figure 9*a* is the computed FM function of Fig. 8*b*; it is estimated by Eqs 25–28. The direction of each arrow (frequency vector) can be obtained by $[\,|v(x, y)|\,/\,|u(x, y)|\,]$.

With the computed FM function (as Fig. 9*a*), we can discriminate between the defective regions and the (relative) complete pattern regions automatically. First, we compute the magnitude of $u(x, y)$ and $v(x, y)$, $\sqrt{[\,|u(x, y)|^2 + |v(x, y)|^2]}$, at each pixel. Second, we use a window (each pixel as the window center) to compute the local mean value of the neighboring pixels' magnitudes. The window is moving pixel by pixel. After the process, we can re-

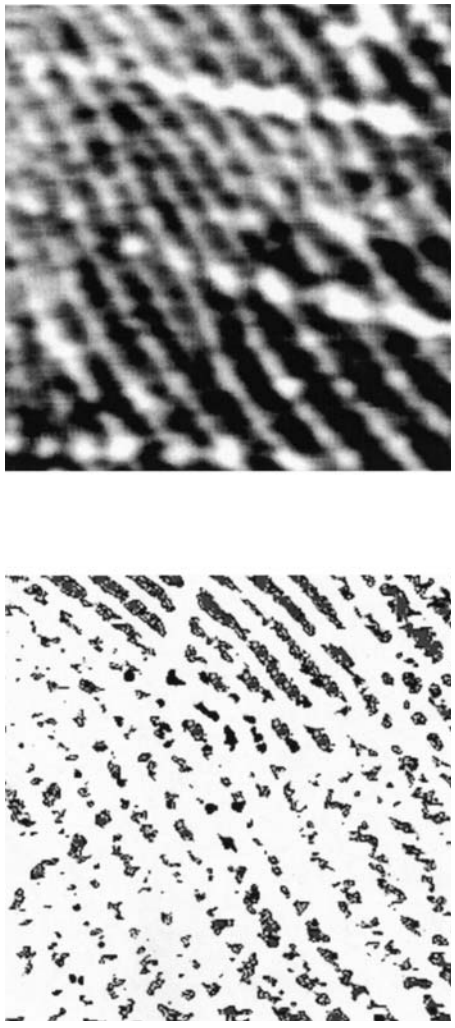

FIG. 8—*(a) An original fingerprint image with similar oriented patterns; (b) the preprocessed image of (a).*

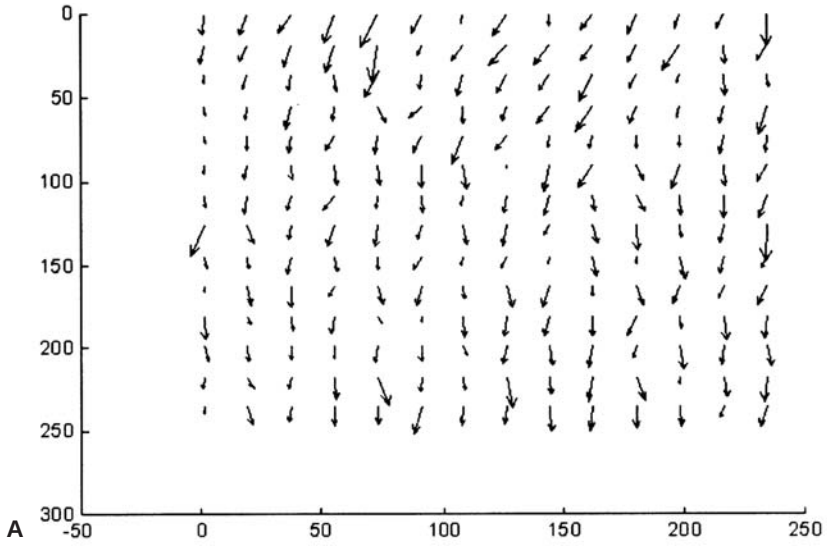

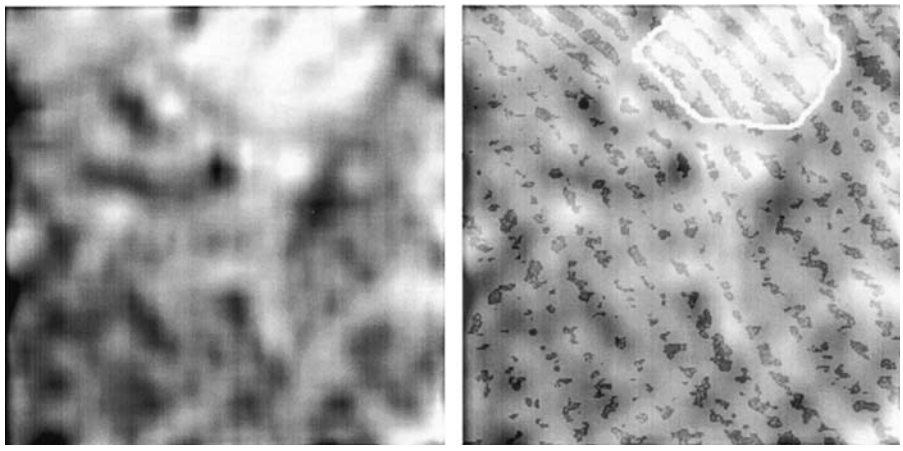

FIG. 9—*(a) The estimated FM function (frequency vectors) of Fig. 8b*; *(b) the local means of FM function*; *(c) the result image of Fig. 8b being superimposed on Fig. 9b. The region surrounded by the white contour is the (relative) complete pattern region.*

place each pixel's gray level values with its neighboring pixel's local mean value. Third, we show the local mean values as an image (as Fig. 9*b*). Finally, we let Fig. 8*b* be superimposed on Fig. 9*b* and show the image as Fig. 9*c*. In Fig. 9*c*, the region surrounded by the white contour is the (relative) complete pattern region.

Experimental Results

Applications to the Surface Textures of Skid-Proof Brick

The processing flowchart of the proposed fingerprint restoration is shown in Fig. 10. In Fig. 11, we use this method to restore the surface textures of skid-proof brick. Figure 11*a* is an original image, Fig. 11*b* is the synthetic image by removing the center information, and Fig. 11*c* is the restored result by the proposed method. From Fig. 11*c*, we can see the restored image is similar to the original one.

Applications to Defective Fingerprint Image Patterns

We apply our method to restore the defective image in Fig. 8*b*. After three iterative processes (i.e., $t = 3$), the discontinuous textures have been connected and restructured (see Fig. 12*a*). Figure 12*b* is the restored image after five iterative processes (i.e., $t = 5$). If the defective fingerprint image is superimposed on a line (e.g., form lines), the image is still restored pretty well. Figure 13*a* is a defective fingerprint image with a black line (contaminated) over it, and Fig. 13*b* is the restored result with our method.

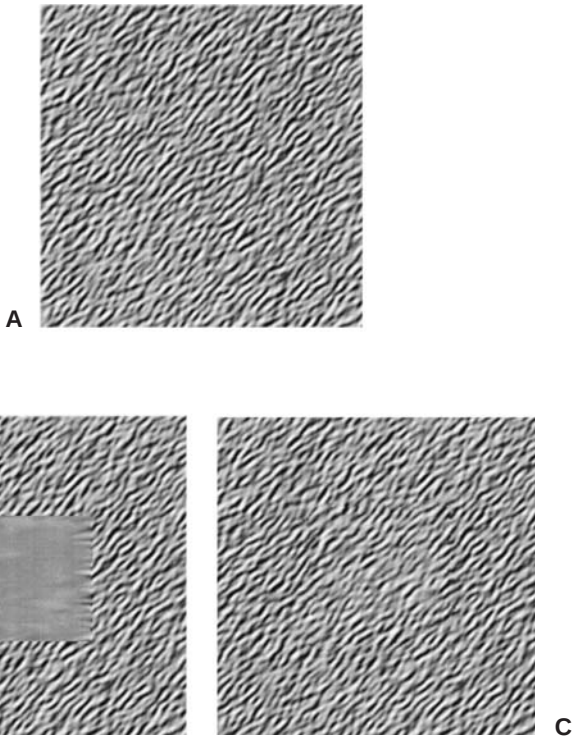

FIG. 11—*The surface textures of skid-proof brick examples*: *(a) an original image*; *(b) the synthetic image by removing its center information*; *(c) the restored result by the proposed method. The restored image is similar to the original one.*

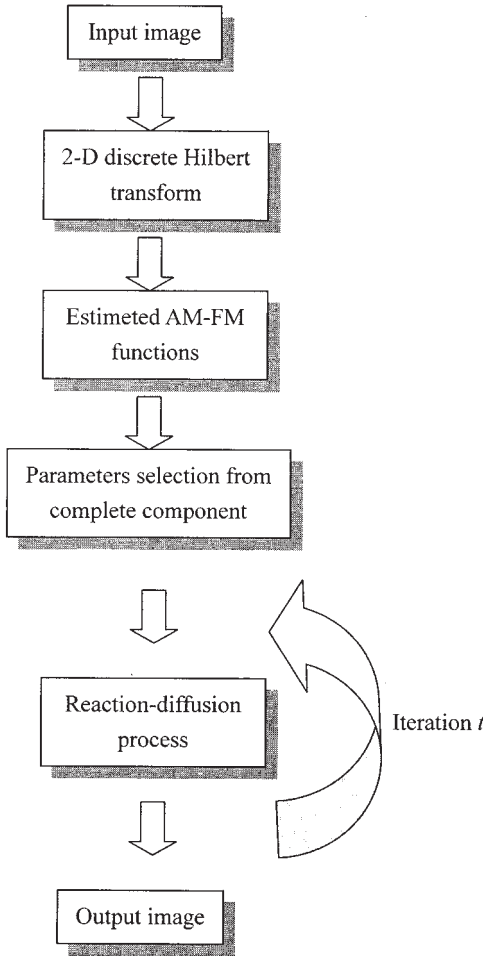

FIG. 10—*The processing flowchart of the proposed fingerprint restoration method.*

The Comparison of Synthetic Completing Fingerprints

Figure 14*a* is an original perfect fingerprint image (the symbols show the feature positions detected by AFIS). Figure 14*b* is the same image processed by the bad impressing process. We can see some "false alarm" features being generated and some features being missed. Figure 14*c* is the restored image by the proposed method. From the experimental results, we can see our method can reduce the extraction of "false alarm" features.

The restoration results by fingerprint examiners and our method are shown in Fig. 15. Figure 15*a* is an original perfect fingerprint image. Figure 15*b* is the same image processed by the bad impressing process. Figure 15*c* and Fig. 15*d* are the restored images by our method and fingerprint examiners, respectively. From the experimental results, we can see the feature extraction results are similar to each other.

Discussion

In this paper, we propose a novel digital image restoration technique based on the AM-FM reaction-diffusion method to restore defective or contaminated fingerprint patterns. We compute a complex-valued extension of processed fingerprint image with Hilbert Transform and estimate the parameters of the AM-FM functions demodulated from the complex-valued extension. In the reaction-diffusion process, the estimated parameters are used to reconstruct fingerprint patterns. Our method shows its potential application to fingerprint pattern enhancement in the recognizing process (but not

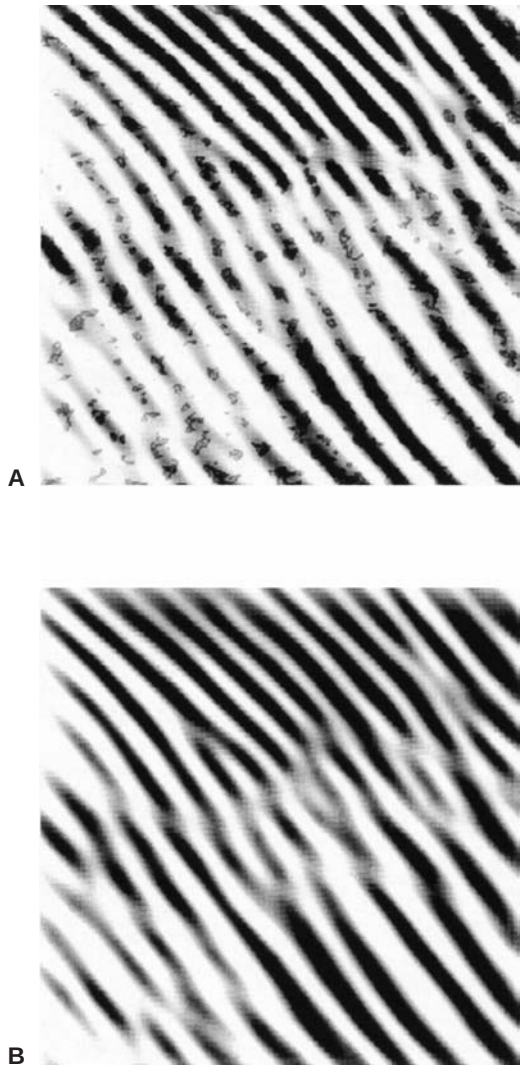

FIG. 12—*The restored result images*: *(a) after three iterative processes (i.e.,), the discontinuous textures have been connected and restructured*; *(b) the restored image after five iterative processes (i.e., $t = 5$).*

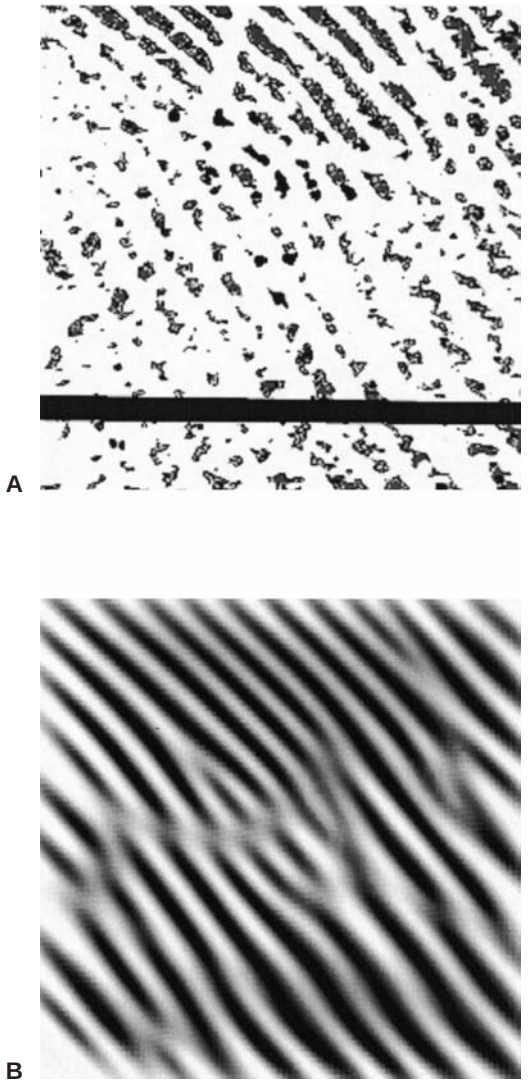

FIG. 13—*If the defective fingerprint image is superimposed on a line (e.g., form lines), the image is still restored pretty well with our method. (a) A defective fingerprint image with a black line over it*; *(b) the restored result.*

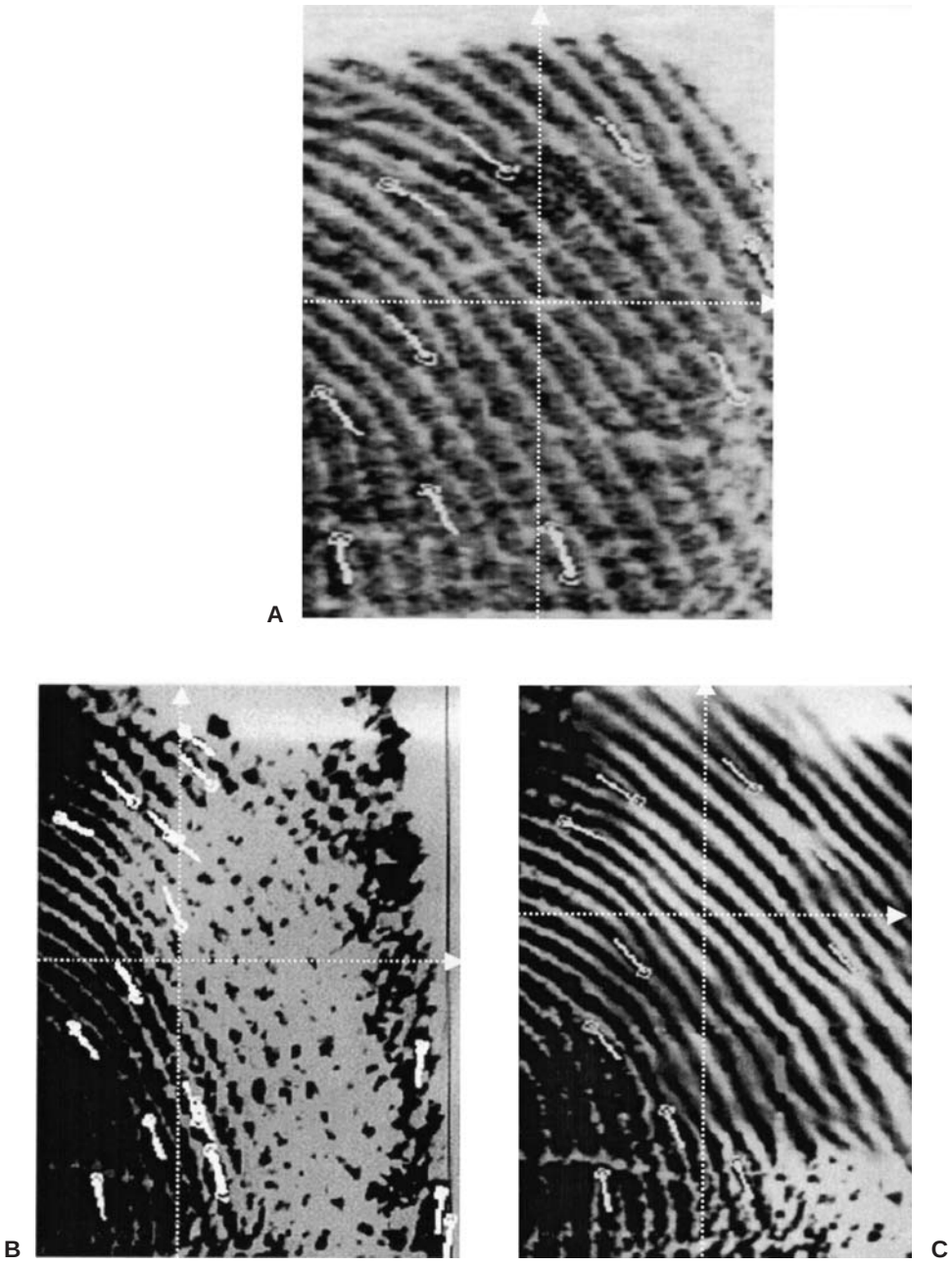

FIG. 14—*A defective fingerprint image restored by the proposed method; the symbols show the feature positions detected by AFIS. (a) The original perfect fingerprint image; (b) the same fingerprint image with the bad impressing process, we can see some "false alarm" features being generated and some features being missed; (c) the restored image by the proposed method.*

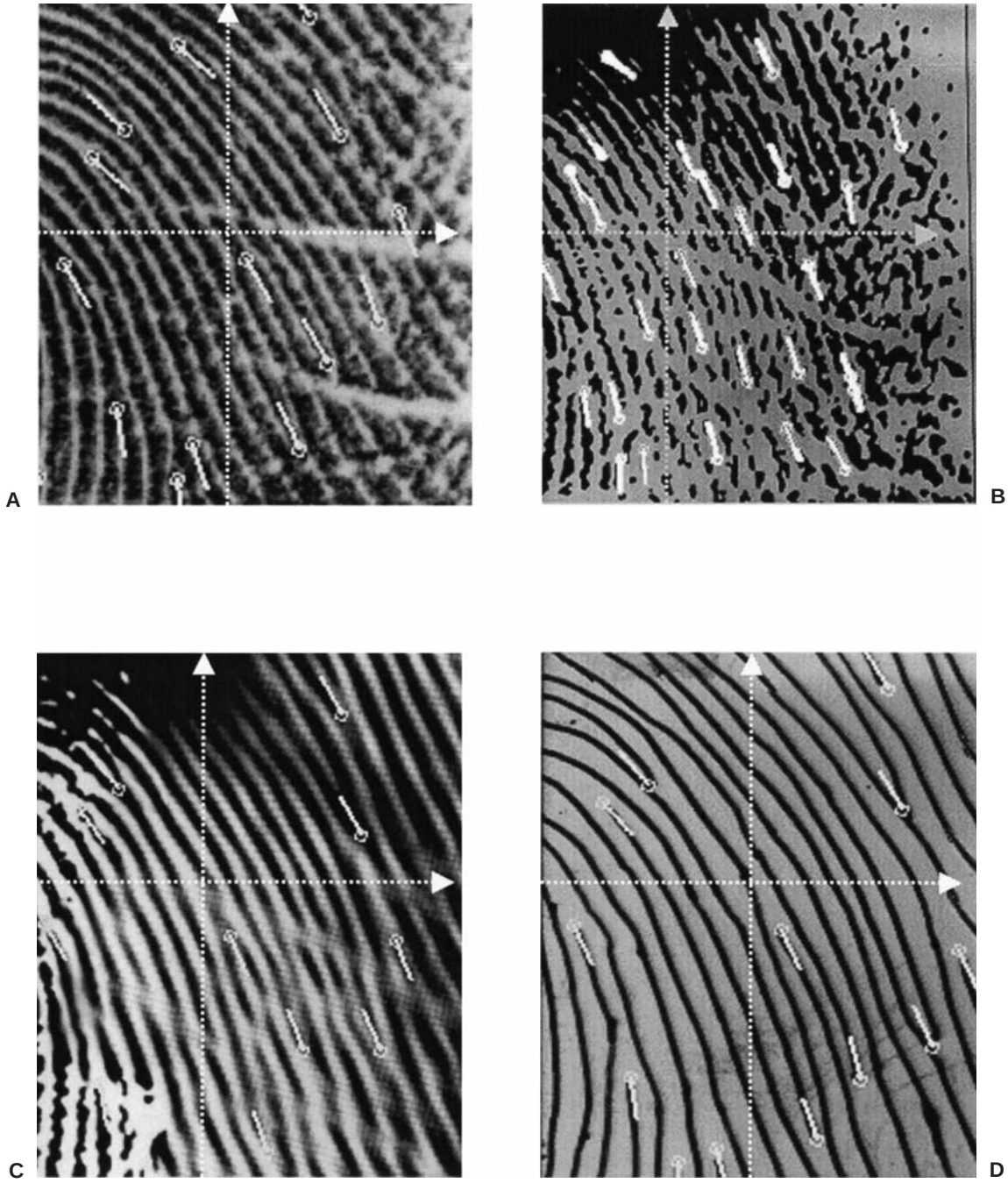

FIG. 15—*(a) An original perfect fingerprint image; (b) the same image with the bad impressing process; (c) and (d) are the restored images by our method and fingerprint examiners, respectively. From the experimental results, we can see the feature extraction results are similar to each other.*

for the identifying process). It can be applied to improving the legibility of input image of automated systems (such as AFIS). Synthetic and real images are used to show the capability of the proposed method. The results of enhancing fingerprint patterns by the manual process and our method are evaluated and compared.

Since our method produce patterns that correspond to "oriented" texture features, it cannot create any specific patterns that are different from those features. When applying the method to fingerprint pattern restoration, one must notice that the size of the poor clarity region cannot be of an order greater than that of the fingerprint ridges; otherwise, one may generate "false alarm features." For example, in Fig. 11, the restored image is "similar" to the original image, but it is not identical to the original image.

Acknowledgments

The authors would like to thank the anonymous reviewers for their insight, comments and valuable suggestions. This work was supported by National Science Council, Taiwan (NSC91-2213-E-015-001) and the Criminal Investigation Bureau, Taiwan.

References

1. John B. The history and development of fingerprinting. In: Henry CL, Gaensslen RE, editors. Advances in fingerprint technology. New York: CRC, 1994;1–38.
2. Vigo GP, Hueber DM, Vo-Dinh T. Evaluation of data techniques for improved analysis of fingerprint images. J Forensic Sci 1995;40(5): 826–37.
3. Moler E, Ballarin V, Pessana F, Torres S, Olmo D. Fingerprint identification using image enhancement techniques. J Forensic Sci 1998; 43(3):689–92.
4. Kaymaz E, Mitra S. A novel approach to Fourier spectral enhancement of laser-luminescent fingerprint images. J Forensic Sci 1993;38(3): 530–41.
5. Acton ST, Havlicek JP, Bovik AC. Oriented texture completion by AM-FM reaction-diffusion. IEEE Trans Image Proc 2001 June;10(6): 885–96.
6. Zhu S, Mumford D. Prior learning and Gibbs reaction-diffusion. IEEE Trans Pattern Anal Machine Intell 1997 Nov;19:1236–50.
7. Turk G. Generating textures on arbitrary surfaces using reaction-diffusion. Computer Grphics 1991;25(4):289–98.
8. Witkin A, Kass M. Reaction-diffusion textures. Computer Graphics 1991;25(4):299–308.
9. Perona P, Malik J. Scale-space and edge detection using anisotropic diffusion. IEEE Trans Pattern Anal Machine Intell 1990;12:629–39.
10. Segall CA, Acton ST. Morphological anisotropic diffusion. IEEE International Conference Image Proc 1997 Oct;348–51.
11. Gonzalez RC. Digital image processing. Addison-Wesley, 1992;548–60.
12. Acton ST. Diffusion-based edge detectors. In: Bovik AC, editor. Handbook of image and video processing. New York: Academic, 2000;433–47.
13. Havlicek JP, Bovik AC. Image modulation models. In: Bovik AC, editor. Handbook of image and video processing. New York: Academic, 2000;313–24.
14. Maragos P, Bovik AC. Demodulation of images modeled by amplitude-frequency modulations using multidimensional energy separation. IEEE International Conference Image Proc 1994;421–5.
15. Maragos P, Kaiser JF, Quatieri TF. Energy separation in signal modulations with application to speech analysis. IEEE Trans Signal Proc 1993 Oct;41(10):3024–51.
16. Lu S, Doerschuk PC. Nonlinear modeling and processing of speech based on sums of AM-FM formant models. IEEE Trans Signal Proc 1996 Apr;44(4):773–82.
17. Maragos P, Kaiser JF, Quatieri TF. On amplitude and frequency demodulation using energy operators. IEEE Trans Signal Proc 1993 Apr; 41(4):1532–50.
18. Vakman D. On the analytic signal, the Teager-Kaiser energy algorithm, and other methods for defining amplitude and frequency. IEEE Trans Signal Proc 1996 Apr;44:791–7.
19. Havlicek JP, Pattichis MS, Harding DS, Christofides AC, Bovik AC. AM-FM image analysis techniques. IEEE Southwest Symposium. Image analysis interpretation, 1996 Apr;195–9.
20. Havlicek JP, Harding DS, Bovik A C. The multicomponent AM-FM image representation. IEEE Trans Image Proc 1996 Jun;l.5:1094–100.
21. Bovik AC, Gopal N, Emmoth T, Restrepo A. Localized measurement of emergent image frequencies by Gabor wavelets. IEEE Trans Inf Theory 1992;38:691–712.
22. Havlicek JP, Harding DS, Bovik AC. The analytic image. IEEE International Conference Image Proc 1997 Oct;446–9.
23. Gabor D. Theory of communication. J Inst Elect Eng 1946;193(3): 429–57.
24. Marple SL. Computing the discrete-time analytic signal via FFT. IEEE Trans Signal Proc 1999 Sep;47:2600–3.
25. Havlicek JP, Havlicek JW, Mamuya ND, Bovik AC. Skewed 2D Hilbert transforms and computed AM-FM models. IEEE International Conference Image Proc 1998 Oct;602–6.
26. Havlicek JP, Harding DS, Bovik AC. Discrete quasieigen-function approximation for AM-FM image analysis. IEEE International Conference Image Proc 1996;633–6.

Additional information and reprint requests:
Che-Yen Wen, Ph.D.
Department of Forensic Science, Central Police University
56 Shu-Ren Road, Kuei-Shan
Taoyuan, Taiwan 33334
Tel: 886-3-3285187
Fax: 886-3-3275907
E-mail: cwen@sun4.cpu.edu.tw